

**Deuterium site occupation in the oxygenstabilized  $\eta$ carbides  $Zr_3V_3O_{12}x$  . I. Preparation and neutron powder diffraction**

F. J. Rotella, H. E. Flotow, D. M. Gruen, and J. D. Jorgensen

Citation: *The Journal of Chemical Physics* **79**, 4522 (1983); doi: 10.1063/1.446339

View online: <http://dx.doi.org/10.1063/1.446339>

View Table of Contents: <http://scitation.aip.org/content/aip/journal/jcp/79/9?ver=pdfcov>

Published by the [AIP Publishing](#)

---

**Articles you may be interested in**

[X-ray diffraction study of aluminum carbide powder to 50 GPa](#)

*J. Appl. Phys.* **106**, 083511 (2009); 10.1063/1.3246808

[Studies of V, Nb, Cr, and Zr substituted 2:17 compounds and their carbides using neutron diffraction](#)

*J. Appl. Phys.* **81**, 4542 (1997); 10.1063/1.365421

[Neutron diffraction and Mössbauer effect study of the preferential silicon site occupation and magnetic structure of  \$Nd\_2Fe\_{14-x}Si\_xB\$](#)

*J. Appl. Phys.* **74**, 6798 (1993); 10.1063/1.355080

[Deuterium site occupation in the oxygenstabilized  \$\eta\$ carbides  \$Zr\_3V\_3O\_{12}x\$  . II. Application of a geometric model](#)

*J. Chem. Phys.* **79**, 4532 (1983); 10.1063/1.446367

[Neutron diffraction studies of  \$Nd\_2\(Co\_xFe\_{1-x}\)\_{17}\$  alloys: Preferential site occupation and magnetic structure](#)

*J. Appl. Phys.* **53**, 250 (1982); 10.1063/1.331601

---



# Deuterium site occupation in the oxygen-stabilized $\eta$ -carbides $Zr_3V_3OD_x$ . I. Preparation and neutron powder diffraction<sup>a)</sup>

F. J. Rotella, H. E. Flotow, D. M. Gruen, and J. D. Jorgensen

Argonne National Laboratory, Argonne, Illinois 60439

(Received 18 April 1983; accepted 29 July 1983)

The structures of the single-phase, well-crystallized family of hydrides  $Zr_3V_3OD_x$  for  $x = 0, 1.86, 2.85,$  and  $4.93$  have been refined by the Rietveld method from neutron powder diffraction data taken at 298 K. The alloy and the three deuterides studied all possess the  $\eta$ -carbide structure (cubic  $Fd\bar{3}m$ ; origin at  $\bar{4}3m$ ). Deuterium is found to occupy four different tetrahedral interstices preferentially. Sites with the largest number of Zr near neighbors appear to fill first unless occupation is hindered by nearby oxygen or simultaneously occupied deuterium sites. The volume expansion per number of deuterium atoms is nearly linear, even though the lowest stable hydride concentration at 298 K is near  $Zr_3V_3OD_{1.5}$  and markedly nonlinear distortions occur within the unit cell as different sites fill.

## INTRODUCTION

A brief account of the synthesis of pure  $Zr_3V_3O$ , developed by one of the present authors, as well as hydrogen absorption properties and equilibrium hydrogen pressures as a function of temperature for compositions between  $Zr_3V_3OH_{1.0}$  and  $Zr_3V_3OH_{4.0}$  were recently reported by Mendelsohn.<sup>1</sup> A detailed structural study of this system is of particular importance because the alloy structure contains an unusually large number of inequivalent interstitial sites which could accommodate hydrogen, and because no complete structural information is available for the hydrides of any of the members of this family.

The alloy  $Zr_3V_3O$  has the  $\eta$ -carbide, or  $Ti_2Ni$ -type, structure (cubic space group  $Fd\bar{3}m$ ) which is common for  $A_2B$  alloys.<sup>2</sup> For some of these alloys oxygen can enter the structure, but is not required for its stability. For example,  $Ti_2Ni$  is cubic with  $a_0 = 11.319 \text{ \AA}$  and its oxygen containing polymorph  $Ti_4Ni_2O$  is isostructural with  $a_0 = 11.328 \text{ \AA}$ .<sup>3</sup> In the zirconium-vanadium system, oxygen is required to stabilize the  $\eta$ -carbide structure  $Zr_3V_3O$ . (Note also that vanadium occupies two kinds of sites, with one of these being a site occupied by Ti in  $Ti_4Ni_2O$ .) The minimum and maximum amounts of oxygen that will stabilize  $Zr_3V_3O_x$  in the  $\eta$ -carbide structure have been found to be 0.6 and 1.0, respectively. Some oxygen-stabilized alloys of this type form hydrides that vary in hydrogen capacity or stability as a function of oxygen content.<sup>1</sup> Thus, it may be possible to systematically modify the properties of these hydrides. However, this paper reports only the hydride structures derived from the stoichiometric alloy  $Zr_3V_3O$ .

Only a few previous attempts to locate hydrogen sites in  $\eta$ -carbide alloys have been reported. Buchner *et al.* considered the possible hydrogen sites in  $Ti_2NiH_x$  from a geometric point of view and compared neutron powder diffraction data with calculated intensities.<sup>4</sup> They obtained reasonable agreement for a model with hydrogen

in high symmetry  $8a$ ,  $8b$ , and  $16d$  sites. Stioui *et al.* performed neutron diffraction measurements on  $Ti_4Fe_2OD_{2.25}$  and analyzed their data with a model consisting of deuterium in  $8a$  sites in the center of titanium octahedra, plus lower symmetry  $96g$  and  $192i$  sites.<sup>5</sup> They found no occupation of the other eight-fold site at the center of Fe tetrahedra which Buchner *et al.* reported to be occupied in  $Ti_2NiH_x$ . Jones, Halstead, and Buschow reported NMR results for  $Hf_2RhH_{2.2}$  and  $Hf_2CoH_{3.8}$  which could be explained only in terms of at least three low symmetry hydrogen sites,  $32e$ ,  $96g$ , and  $192i$ .<sup>6</sup> Unfortunately, none of these studies represents a truly exhaustive search for, and an unconstrained refinement of, the hydrogen positions in an  $\eta$ -carbide structure.

The purpose of this paper is to report full structural refinements of the  $\eta$ -carbide  $Zr_3V_3OD_x$  structure over a wide range of deuterium concentration. In the initial stages of refinement, all geometrically possible deuterium sites are simultaneously allowed. The sum of deuterium occupancies is unconstrained so that the total refined deuterium content can be compared with the analytically determined concentration as a strict test of the structural model. As the total deuterium concentration increases, a clear sequence of site filling obtains and internal structural modifications of the  $Zr_3V_3O$  framework depend markedly on the sites being filled.

## PREPARATION AND CHARACTERIZATION OF SAMPLES

The  $Zr_3V_3O$  sample was prepared from zirconium and vanadium metal powders and  $V_2O_5$ . The zirconium powder was prepared by reacting zirconium rods with hydrogen to produce  $ZrH_2$  which was then crushed and ground to a fine powder in an agate mortar. The  $ZrH_2$  powder was thermally decomposed to produce zirconium metal in a slightly sintered form, which was then ground to a powder. Vanadium powder was prepared from  $VH_{0.8}$  in a manner analogous to that described for zirconium. The  $V_2O_5$  (J. T. Baker analyzed grade) was heated to 1023 K in a flowing stream of oxygen to assure

<sup>a)</sup>Work supported by the U.S. Department of Energy.

TABLE I. Analyses of materials used to prepare  $Zr_3V_3O$ . Impurities are in ppm by weight.<sup>a</sup>

Sample	Metal Impurities	O	N	C
Zr	<250	102	19	171
V	<200	1560	70	60
$V_2O_5$	<200	...	...	...

<sup>a</sup>Metal impurities determined by spectrometric analysis, the others by inert gas fusion.

proper stoichiometry.<sup>7</sup> These starting materials were tested for metal impurities by spectrometric analyses and for nonmetal impurities by chemical analyses; the results are presented in Table I. These impurity levels are believed to be too low to affect the results reported in this paper.

The metal powders and hydrides were manipulated in a glove box filled with purified helium (<10 ppm  $H_2O$  and  $O_2$ ) and were never exposed to air. Likewise, the preparation of  $Zr_3V_3O$  was carried out in an inert atmosphere or in a diffusion-pumped vacuum system.

Weighed amounts of Zr, V, and  $V_2O_5$  were mixed and pressed to form a compact cylinder that was heated to 970 K in vacuum in order to melt the  $V_2O_5$ . The latter step was deemed necessary to prevent loss of oxygen in the next preparation step, which was arc melting the cylinder in an argon atmosphere. Two arc-melted buttons, each weighing 4 g, were made. Preliminary experiments showed that high temperature annealing was required to produce a single phase sample. Consequently, each of the buttons was annealed in an evacuated quartz tube at 1450 K for 280 h. X-ray powder patterns indicated the presence of a single, cubic phase with  $a_0 = 12.168 \pm 0.003$  Å. Polished specimens were examined in a scanning electron microscope (SEM)

at a magnification of 650 ×. Dot patterns (from x radiation) showing the distribution of Zr or V indicated that each element was uniformly dispersed in the samples; dot patterns before annealing showed a nonuniform Zr and V distribution. Both the x-ray powder patterns and the SEM dot patterns indicated that the two  $Zr_3V_3O$  buttons were single-phase samples. The two batches were broken up and combined.

The amount of oxygen in the sample after annealing was found by the inert gas fusion technique to correspond to the composition  $Zr_3V_3O_{1.01 \pm 0.03}$ . The amounts of Zr and V were determined from the weighed amounts of these elements used in the alloy preparation.

The deuteride samples were prepared by direct reaction of deuterium with  $Zr_3V_3O$ . The deuterium was stored as, and generated by thermal decomposition of,  $UD_3$ . The only significant impurity in the deuterium was 0.5% hydrogen. The first deuteride made, which had the composition  $Zr_3V_3OD_{4.64}$ , was thermally decomposed at 923 K to regenerate the alloy in the form of a fine powder. The alloy sample (~6.6 g) was then put into a vanadium capsule and neutron diffraction data were taken.

Subsequently, the alloy sample near 300 K was reacted with deuterium to produce the compositions  $Zr_3V_3OD_x$ , where  $x = 1.05 \pm 0.01$ ,  $1.86 \pm 0.02$ ,  $2.85 \pm 0.02$ , and  $4.93 \pm 0.03$ . For each composition the amount of deuterium reacted was determined volumetrically before and after the neutron diffraction data were taken. All the deuterides had a negligible deuterium pressure at room temperature except  $Zr_3V_3OD_{4.93}$  which had a pressure of about 0.3 Torr.

## NEUTRON DIFFRACTION

The neutron diffraction data were collected on the special environment powder diffractometer (SEPD) at

TABLE II. Summary of the Rietveld analyses for  $Zr_3V_3OD_x$ .

$x$	0.0	1.86	2.85	4.93
Crystal system		Cubic		
Space Group		$Fd\bar{3}m$ (origin at $\bar{4}3m$ )		
$a$ (Å)	12.1703(1)	12.3175(1)	12.3807(1)	12.5260(1)
$V$ (Å <sup>3</sup> )	1802.62(4)	1868.82(4)	1897.72(4)	1965.35(4)
$Z$		16		
Formula weight	442.49	446.25	448.25	452.46
Calculated density (g cm <sup>-3</sup> )	6.521	6.343	6.275	6.116
$d$ range (Å)	0.42–2.34	0.42–2.51	0.42–2.38	0.42–2.41
Number of observations	2375	2482	2414	2411
Number of reflections	660	677	695	711
Number of variables	13	18	27	35
$R_{p2}$ (%) <sup>a</sup>	6.15	5.74	6.54	9.22
$R_p$ (%) <sup>a</sup>	2.14	2.00	1.99	1.91
$R_{wp}$ (%) <sup>a</sup>	3.24	3.29	2.94	2.69
$R_{exp}$ (%) <sup>a</sup>	1.95	1.69	2.04	1.74

<sup>a</sup>These quantities are defined in H. M. Rietveld, *J. Appl. Crystallogr.* **2**, 65 (1969); J. D. Jorgensen and F. J. Rotella, *ibid.* **15**, 27 (1982).

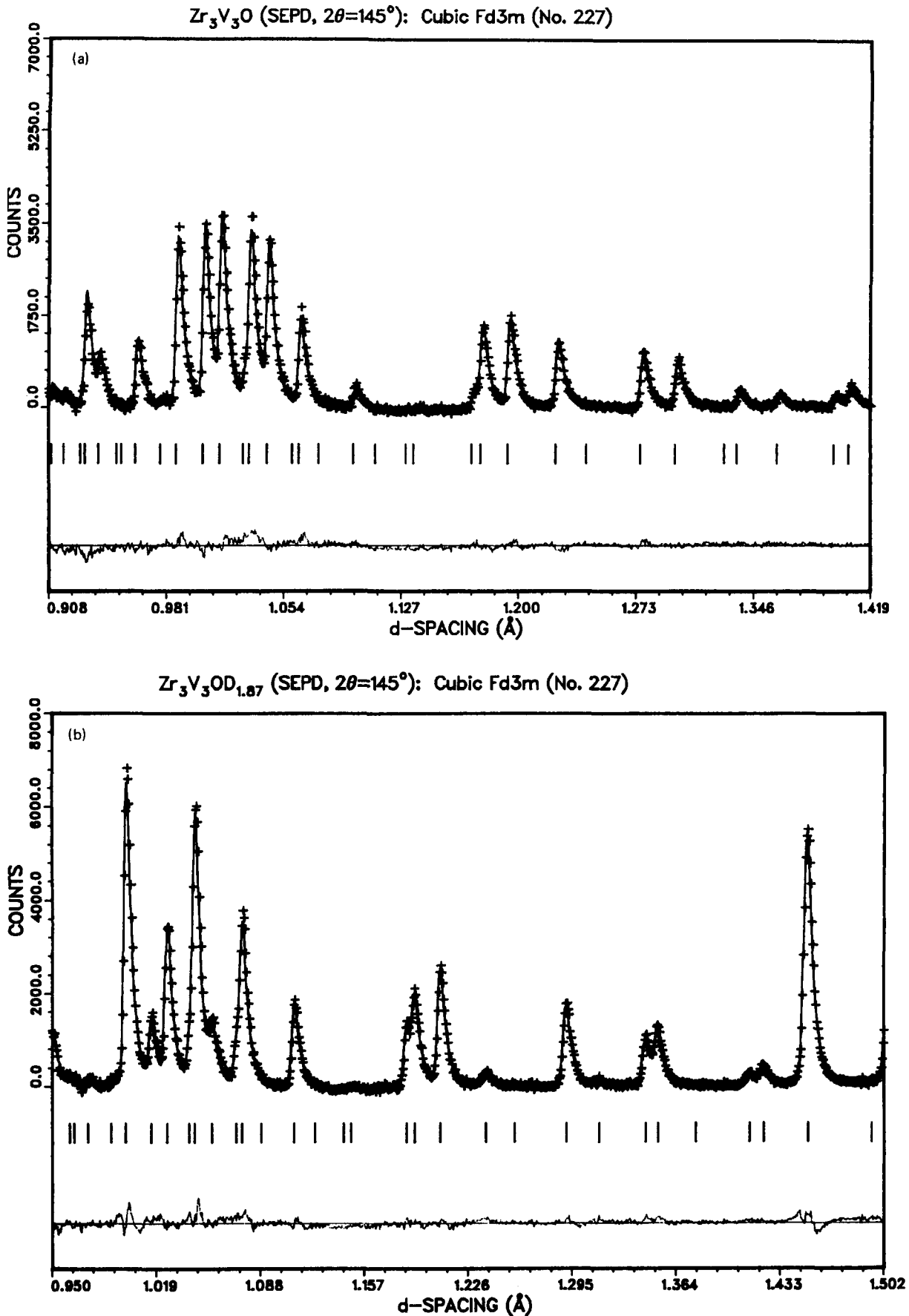


FIG. 1. A portion of the raw diffraction data (+) and Rietveld profile (line) covering the approximate range of  $0.9 < d < 1.5$  Å, for each of the four  $Zr_3V_3OD_x$  samples studied. Tick marks below the data indicate the positions of allowed Bragg reflections used in the calculation. The curve at the bottom of the figure shows the difference between the observed data and the calculation. Background has been subtracted before plotting. (a)  $x=0$ ; (b)  $x=1.86$ ; (c)  $x=2.85$ ; and (d)  $x=4.93$ .

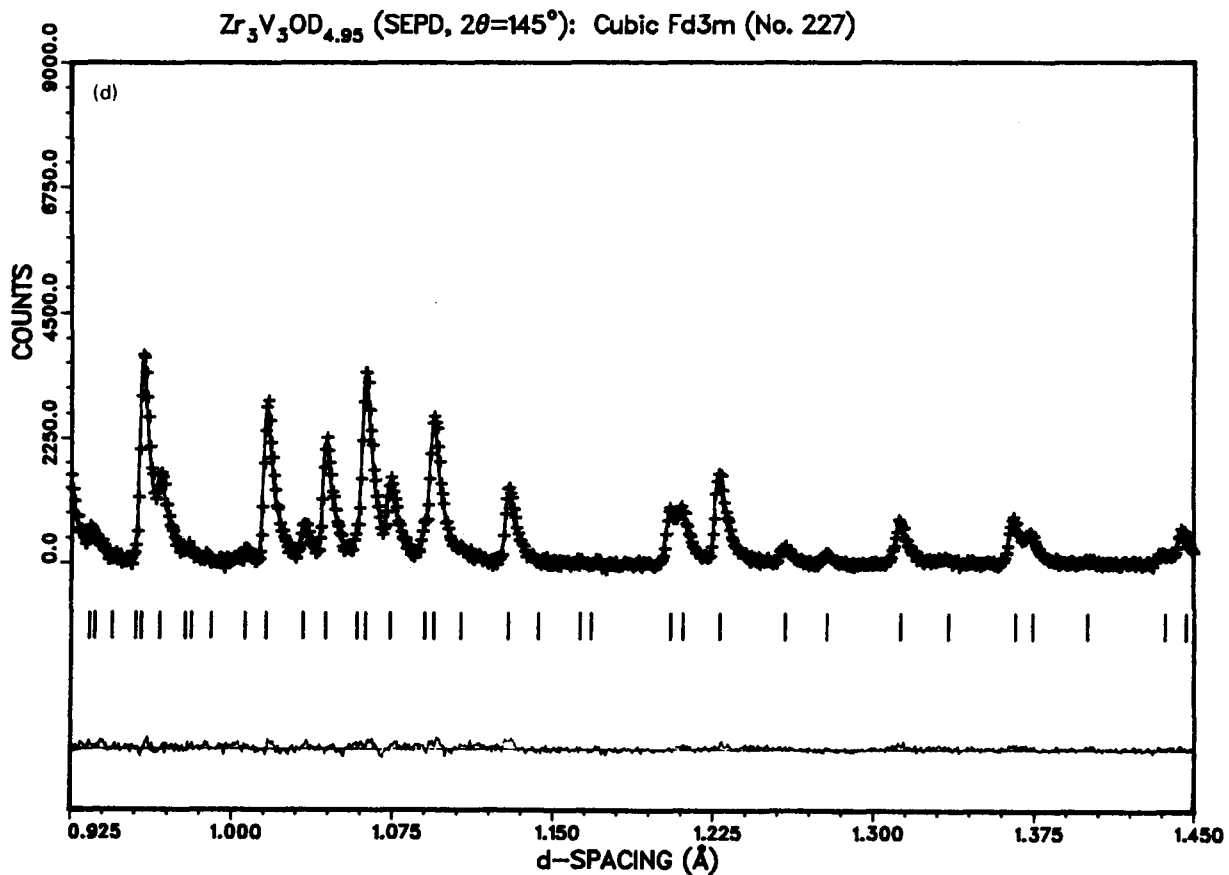
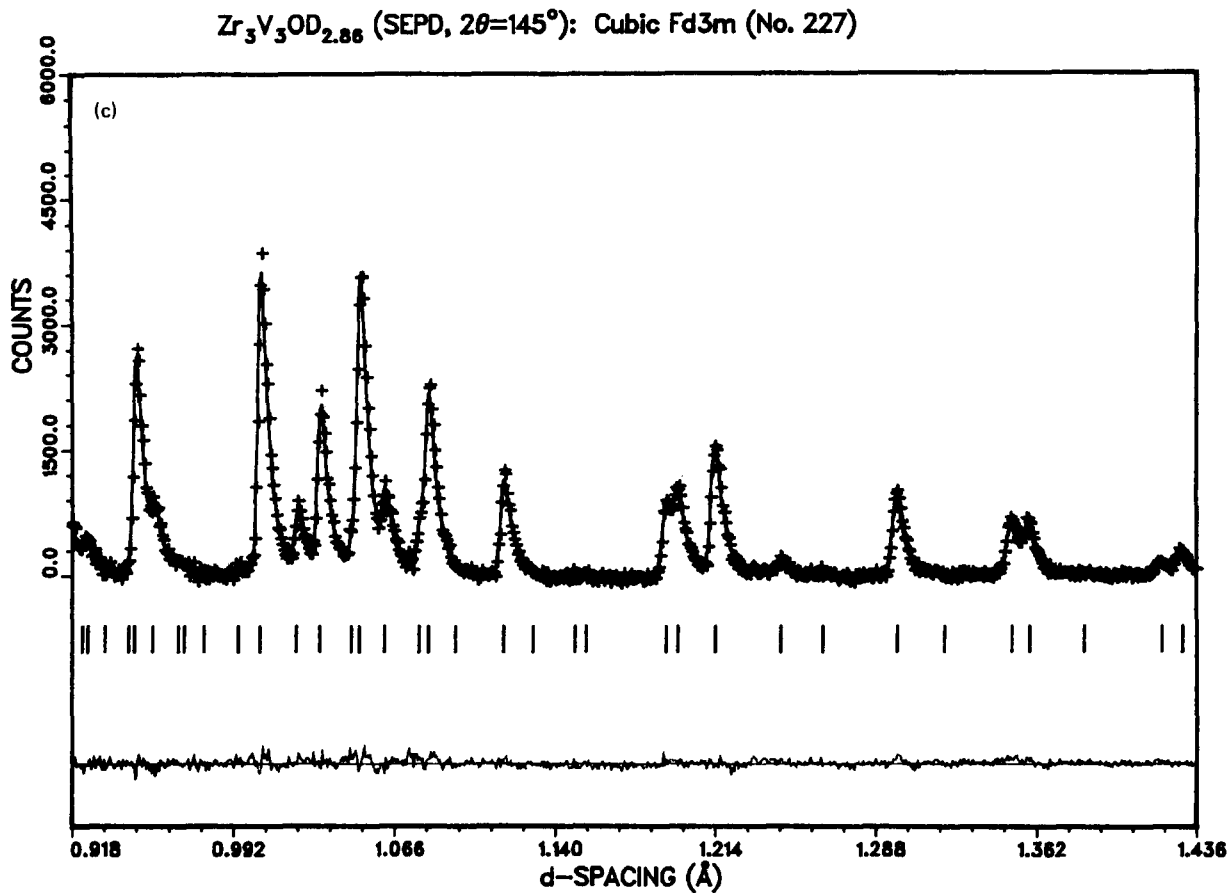


FIG. 1. (Continued)

TABLE III. Positional and thermal parameters from the Rietveld analyses for  $Zr_3V_3OD_x$ .<sup>a,b</sup>

$x$		0	1.86	2.85	4.93
Atom/site	Parameter				
Zr (48f)	Occupancy	3.0	3.0	3.0	3.0
	$x$	0.18959(7)	0.19601(7)	0.19555(8)	0.19424(10)
	$y = z$	0	0	0	0
	$B_{iso}$	0.395(13)	0.271(13)	0.412(15)	0.323(15)
V1 (16d)	Occupancy	1.0	1.0	1.0	1.0
	$x = y = z$	5/8	5/8	5/8	5/8
	$B_{iso}$	0.3	0.3	0.3	0.3
V2 (32e)	Occupancy	2.0	2.0	2.0	2.0
	$x = y = z$	0.8328(8)	0.8260(9)	0.8284(9)	0.8302(10)
	$B_{iso}$	0.3	0.3	0.3	0.3
O (16c)	Occupancy	0.971(11)	0.978(12)	0.948(13)	0.980(14)
	$x = y = z$	1/8	1/8	1/8	1/8
	$B_{iso}$	0.36(3)	0.22(3)	0.42(4)	0.30(4)
D1 (32e)	Occupancy		1.803(20)	1.940(23)	1.995(25)
	$x = y = z$		0.91258(8)	0.91236(7)	0.91202(10)
	$\beta_{11} = \beta_{22} = \beta_{33}$		0.00146(7)	0.00179(7)	0.00182(9)
	$\beta_{12} = \beta_{13} = \beta_{23}$		0.00024(4)	0.00017(4)	0.0020(5)
	$B_{iso}$		1.3 <sup>c</sup>		
D2 (192i)	Occupancy		0.071(21)	0.92(4)	2.65(4)
	$x$		0.7464 <sup>c</sup>	0.7464(7)	0.7490(3)
	$y$		0.8644 <sup>c</sup>	0.8644(7)	0.8616(2)
	$z$		0.9449 <sup>c</sup>	0.9449(7)	0.9429(2)
	$B_{iso}$		1.3 <sup>c</sup>		
	$\beta_{11}$			0.0015(4)	0.00149(18)
	$\beta_{22}$			0.0023(5)	0.00149(15)
	$\beta_{33}$			0.0025(5)	0.00124(16)
	$\beta_{12}$			-0.0009(4)	-0.00078(16)
	$\beta_{13}$			-0.0013(3)	-0.00066(11)
D3 (96g)	Occupancy				0.16(4)
	$x = y$				0.906(3)
	$z$				0.280(4)
	$B_{iso}$				1.4(10)
	$B_{iso}$				1.4(10)
D4 (96g)	Occupancy				0.15(3)
	$x = y$				0.968(2)
	$z$				0.657(3)
	$B_{iso}$				0.7(7)

<sup>a</sup>Esds's, shown in parentheses, are right adjusted to the last digit of the preceding number. They are derived from the inverse of the final least-squares matrix.

<sup>b</sup>Isotropic thermal parameters are in units of  $\text{\AA}^2$ . Anisotropic thermal parameters enter the calculated structure factor expression in the form:

$$\exp[-(h^2\beta_{11} + k^2\beta_{22} + l^2\beta_{33} + 2hk\beta_{12} + 2hl\beta_{13} + 2kl\beta_{23})].$$

<sup>c</sup>These values were taken from the  $x = 2.85$  refinement and fixed throughout this refinement; the value for  $B_{iso}$  represents an "equivalent isotropic thermal parameter" calculated from the associated anisotropic parameters.

Argonne's Intense Pulsed Neutron Source. The SEPD is a time-of-flight diffractometer on a 14 m incident flight path. Detectors are located in electronically time-focused arrays at nominal scattering angles of  $2\theta = \pm 145^\circ$ ,  $\pm 90^\circ$ ,  $\pm 57^\circ$ , and  $\pm 22^\circ$ .<sup>8</sup> The structural refinements were performed with the data collected at  $2\theta = \pm 145^\circ$ , where resolution is the highest. Data from the other angles were used to confirm cell indexing and to confirm that no impurities or second phases were present. Data collection times were 19 h for  $Zr_3V_3O$ , 17 h for  $Zr_3V_3OD_{1.86}$ , 15 h for  $Zr_3V_3OD_{2.85}$ , and 14 h for  $Zr_3V_3OD_{4.93}$ .

The data were analyzed with a Rietveld refinement

technique,<sup>9</sup> modified for use with time-of-flight data from a pulsed neutron source.<sup>10</sup> A summary of the refinement conditions for the data from the four samples studied is given in Table II. In addition to the structural variables, the list of refined parameters included a scale factor, two background parameters, corrections for absorption and extinction, and two peak shape parameters. Some peak broadening was observed, but to a much lesser degree than is normally present in metal hydrides; moreover, the small broadening was nicely modeled by the peak shape function available in the refinement code. The quality of the refinement is evidenced by the observed  $R$  values (Table II). A section of the raw data and calculated profile for each deuterium

TABLE IV. Independent distances ( $\text{\AA}$ ), angles ( $^\circ$ ), and esd's in  $Zr_3V_3OD_x$ .<sup>a</sup>

$x$	0	1.86 <sup>b</sup>	2.85	4.93
(a) Distances from zirconium to zirconium, vanadium, and oxygen				
Zr-Zr (intraoctahedral)	3.2631(12)	3.4144(12)	3.4239(14)	3.4409(18)
Zr-Zr (interoctahedral)	3.2153(4)	3.2198(4)	3.2387(4)	3.2836(5)
Zr-V1	3.1178(6)	3.0987(6)	3.1187(7)	3.1670(9)
Zr-V2	2.891(13)	3.043(14)	3.019(15)	3.023(17)
Zr-V2	3.115(3)	3.105(3)	3.117(3)	3.162(4)
Zr-O	2.2905(3)	2.3466(3)	2.3565(4)	2.3781(5)
(b) Distances from vanadium to vanadium and oxygen				
V1-V2	2.631(6)	2.619(5)	2.647(6)	2.690(7)
V2-V2 (intratetrahedral)	2.85(3)	2.65(3)	2.75(3)	2.84(4)
V2-O	3.630(13)	3.781(14)	3.761(14)	3.776(17)
(c) Distances involving deuterium				
D1-Zr		2.0268(7)	2.0346(7)	2.0495(10)
D1-V1		3.6022(12)	3.6173(11)	3.6545(16)
D1-V2		1.85(2)	1.80(2)	1.77(2)
D1-O		2.6971(6)	2.7127(5)	2.7472(8)
D1-D1		3.046(3)	3.069(2)	3.117(4)
D1-D2		2.168	2.176(8)	2.172(3)
D1-D3				3.31(4)
D1-D4				2.928(8)
D2-Zr		1.937	1.949(10)	2.005(3)
D2-Zr		1.947	1.961(5)	1.988(2)
D2-V1		1.731	1.740(8)	1.779(3)
D2-V2		1.825	1.819(10)	1.784(6)
D2-O		2.728	2.742(8)	2.778(3)
D2-D2		0.935	0.940(19)	1.049(7)
D2-D2		1.404	1.411(10)	1.440(5)
D2-D2		1.930	1.940(16)	1.960(6)
D2-D2		1.893	1.903(11)	1.981(5)
D2-D2		2.054	2.065(17)	1.995(7)
D2-D2		2.774	2.789(8)	2.797(6)
D2-D3				1.26(3)
D2-D3				2.01(3)
D2-D3				2.19(3)
D2-D4				1.16(2)
D2-D4				1.78(4)
D2-D4				1.91(3)
D2-D4				2.13(2)
D3-Zr				1.98(5)
D3-Zr				2.05(3)
D3-V1				3.02(3)
D3-V2				1.77(5)
D3-O				2.01(5)
D3-D3				2.24(8)
D3-D3				2.33(7)
D3-D4				1.93(6)
D3-D4				2.81(4)
D3-D4				2.94(4)
D4-Zr				1.95(4)
D4-V1				1.69(4)
D4-V2				1.81(3)
D4-O				3.56(3)
D4-D4				1.15(8)
D4-D4				2.20(6)
(d) Angles centered on deuterium				
Zr-D1-Zr		114.77(4)	114.58(3)	114.16(5)
V2-D1-Zr		103.44(5)	103.69(5)	104.24(6)
Zr-D2-Zr		112.0	111.8(4)	110.63(14)
V1-D2-Zr		114.7	114.7(4)	114.30(15)
V1-D2-Zr		115.2	115.3(4)	113.49(16)
V1-D2-V2		94.8	96.1(6)	98.1(6)
V2-D2-Zr		107.9	106.4(7)	105.7(7)
V2-D2-Zr		110.8	111.1(4)	113.83(19)

TABLE IV (Continued)

$x$	4.93
(d) Angles centered on deuterium	
Zr-D3-Zr	109.3(15)
Zr-D3-Zr	114(2)
Zr-D3-O	71.7(14)
Zr-D3-O	73.1(16)
V2-D3-Zr	104.5(16)
V2-D3-Zr	115(3)
V2-D3-O	172(5)
V1-D4-Zr	121(2)
V1-D4-V2	100.5(14)
V2-D4-Zr	114.4(15)
V2-D4-V2	104(3)

<sup>a</sup>Esd's shown in parentheses, are right adjusted to the last digit of the preceding number, and include the effects of the full positional covariance matrix and the uncertainties in the unit cell parameters. No corrections were applied for the possible effects of thermal motion.

<sup>b</sup>See footnote c of Table III.

concentration appears in Fig. 1.

Starting values for atom positions of the alloy  $Zr_3V_3O$  were taken from the literature.<sup>5</sup> It should be noted that some confusion concerning the  $\eta$ -carbide structure exists in the literature due to different choices of unit cell origin. A summary of these different descriptions and their relation to one another has been given by Parthe, Jeitschko, and Sadagopan.<sup>11</sup> As noted in Table II, the origin was taken to be at  $43m$  in the present work. Starting values for the positions of the possible deuterium sites were taken from Didisheim who identified six possible tetrahedral interstices which could accommodate hydrogen in the analogous  $Zr_3V_3N$  structure.<sup>12</sup> The deuterium positions were initially held fixed, and the occupancies allowed to vary. Subsequently, the positions, occupancies, and temperature factors were refined for those sites which exhibited

nonzero occupancy. For deuterium sites with large occupancy, it was possible to refine components of the anisotropic thermal tensor. Conversely, when site occupancy approached zero, e.g.,  $n(D2)$  in  $Zr_3V_3OD_{1.86}$ , it was necessary to hold the positional and thermal parameters fixed while occupancy was refined. The small coherent neutron cross section of vanadium also made it impossible to refine the temperature factors of the two vanadiums, V1 and V2. The final refined structural parameters are listed in Table III. The total deuterium stoichiometries obtained from these unconstrained refinements were 1.87(3) for  $Zr_3V_3OD_{1.86}$ , 2.86(5) for  $Zr_3V_3OD_{2.85}$ , and 4.95(7) for  $Zr_3V_3OD_{4.93}$ , which are in good agreement with the chemically determined deuterium concentrations.

To test whether the small D2 occupation in  $Zr_3V_3OD_{1.86}$  and the small D3 and D4 occupations in  $Zr_3V_3OD_{4.93}$  were truly significant, refinements were undertaken in which the D2 site in the  $x=1.86$  compound and the D3 and D4 sites in the 4.93 compound were held empty, and the weighted profile  $R$  factors ( $R_{wp}$ ) from these refinements were compared with those from the analogous unconstrained refinements using the Hamilton  $R$ -factor ratio test.<sup>13</sup> In the  $x=1.86$  compound, the unconstrained refinement [18 variables;  $n(D2)=0.071(21)$ ] converged to  $R_{wp}=3.2910\%$ , while the constrained refinement [17 variables;  $n(D2)=0$ ] converged to  $R_{wp}=3.3008\%$ . The Hamilton  $R$ -factor ratio indicated that for the unconstrained refinement to be statistically preferred over the constrained refinement at a 99.5% confidence level,  $R_{wp}$  must be lowered by at least a factor of  $(R_{b=1, N=2465, \alpha=0.005}) 1.0016$ .<sup>13</sup> The observed  $R$ -factor ratio is 1.0030, indicating that occupation of the D2 site in the  $x=1.86$  compound is significant at greater than a 99.5% level of confidence. In the  $x=4.93$  compound, the unconstrained refinement [35 variables;  $n(D3)=0.15(4)$  and  $n(D4)=0.15(3)$ ] converged to  $R_{wp}=2.6944\%$ , while the constrained refinements [27 variables;  $n(D3)=0$  and  $n(D4)=0$ ] converged to  $R_{wp}=2.7619\%$ . The

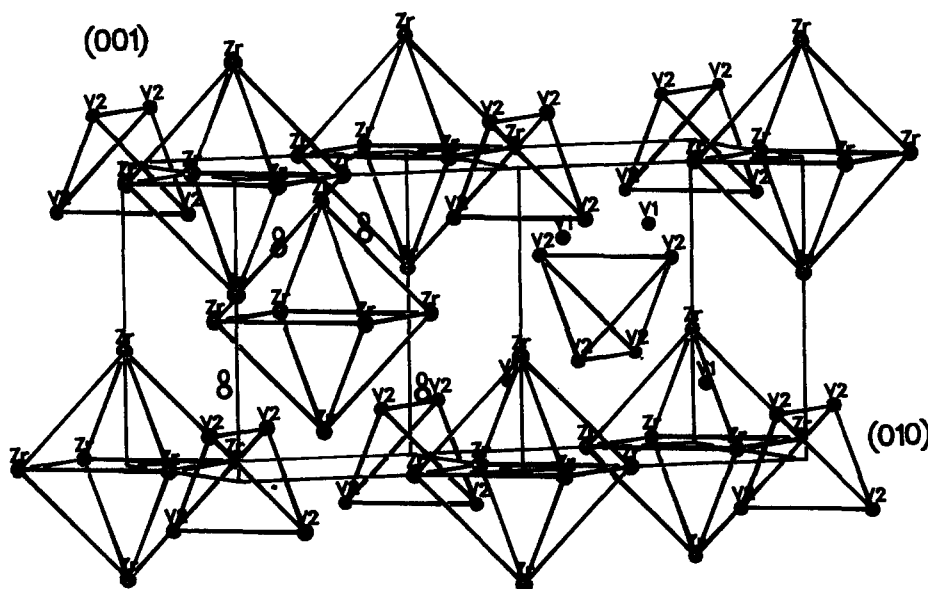


FIG. 2. One-fourth of a unit cell of the alloy  $Zr_3V_3O$  viewed approximately along the (100) direction (ORTEP-II drawing, 50% equiprobability thermal ellipsoids).

TABLE V. Deuterium site occupation ( $n$ ) vs stoichiometry ( $x$ ) in  $Zr_3V_3OD_x$ .

$x_{analytic}$	$x_{refined}$	$n[D1]$	$n[D2]$	$n[D3]$	$n[D4]$
1.86(2)	1.87(3)	1.80(2)	0.07(2)		
2.85(2)	2.86(5)	1.94(2)	0.92(4)		
4.93(3)	4.95(6)	2.00(2)	2.65(4)	0.16(4)	0.15(3)

Hamilton  $R$ -factor ratio at a 99.5% confidence level ( $\mathcal{R}_{b=7, N=2384, \alpha=0.005}$ ) is 1.0043.<sup>13</sup> The observed  $R$ -factor ratio is 1.0251, indicating that occupation of the D3 and D4 sites in the  $x=4.93$  compound is significant at greater than a 99.5% level of confidence.

Independent distances, angles, and associated esd's from  $Zr_3V_3OD_x$  as a function of deuterium composition are collected in Table IV.

### DESCRIPTION OF THE STRUCTURE

The structure of the alloy  $Zr_3V_3O$  is illustrated in Fig. 2. Regular octahedra of zirconium are centered at the  $8a$  sites of  $Fd\bar{3}m$  at  $(0, 0, 0)$ ,  $(1/2, 1/2, 0)$ ,  $(0, 1/2, 1/2)$ ,  $(1/2, 0, 1/2)$ ,  $(1/4, 1/4, 1/4)$ ,  $(3/4, 3/4, 1/4)$ ,  $(1/4, 3/4, 3/4)$ , and  $(3/4, 1/4, 3/4)$ , and regular tetrahedra of vanadium (V2) atoms are centered at the  $8b$  sites,  $(1/2, 1/2, 1/2)$ ,  $(0, 0, 1/2)$ ,  $(1/2, 0, 0)$ ,  $(0, 1/2, 0)$ ,  $(3/4, 3/4, 3/4)$ ,  $(1/4, 1/4, 3/4)$ ,  $(3/4, 1/4, 1/4)$ , and

$(1/4, 3/4, 1/4)$ . The additional vanadium (V1) atoms are located at the  $16d$  sites  $(5/8, 5/8, 5/8)$ ,  $(5/8, 7/8, 7/8)$ ,  $(7/8, 5/8, 7/8)$ , and  $(7/8, 7/8, 5/8)$  plus face centering translations, and the oxygens are on the  $16c$  sites  $(1/8, 1/8, 1/8)$ ,  $(1/8, 3/8, 3/8)$ ,  $(3/8, 1/8, 3/8)$ , and  $(3/8, 3/8, 1/8)$  plus face centering translations. Thus, oxygen is octahedrally coordinated by zirconium, although the octahedron is not regular.

As the alloy absorbs deuterium over the range of concentration from 1.86 to 4.93 atoms per formula unit, four interstices are found to be preferentially occupied by deuterium atoms. These four sites show approximate tetrahedral coordination to zirconium and vanadium atoms. The amount of deuterium in each of these sites for each of the deuterides studied is given in Table V; the sum of the deuterium site occupancies agree extremely well with that determined analytically, indicating that all deuterium sites have been accounted for in each compound. Figure 3 depicts the local environments of each of the four observed deuterium sites. A model explaining the reasons for the observed site preferences appears in a companion paper.<sup>14</sup>

The first site to fill D1, is coordinated by three zirconium atoms comprising a face of a regular octahedron and one vanadium (V2) atom (Fig. 3). It appears that this site almost completely fills ( $n=2$ ) before any other interstice begins to fill; in  $Zr_3V_3OD_{1.88}$ , refined occu-

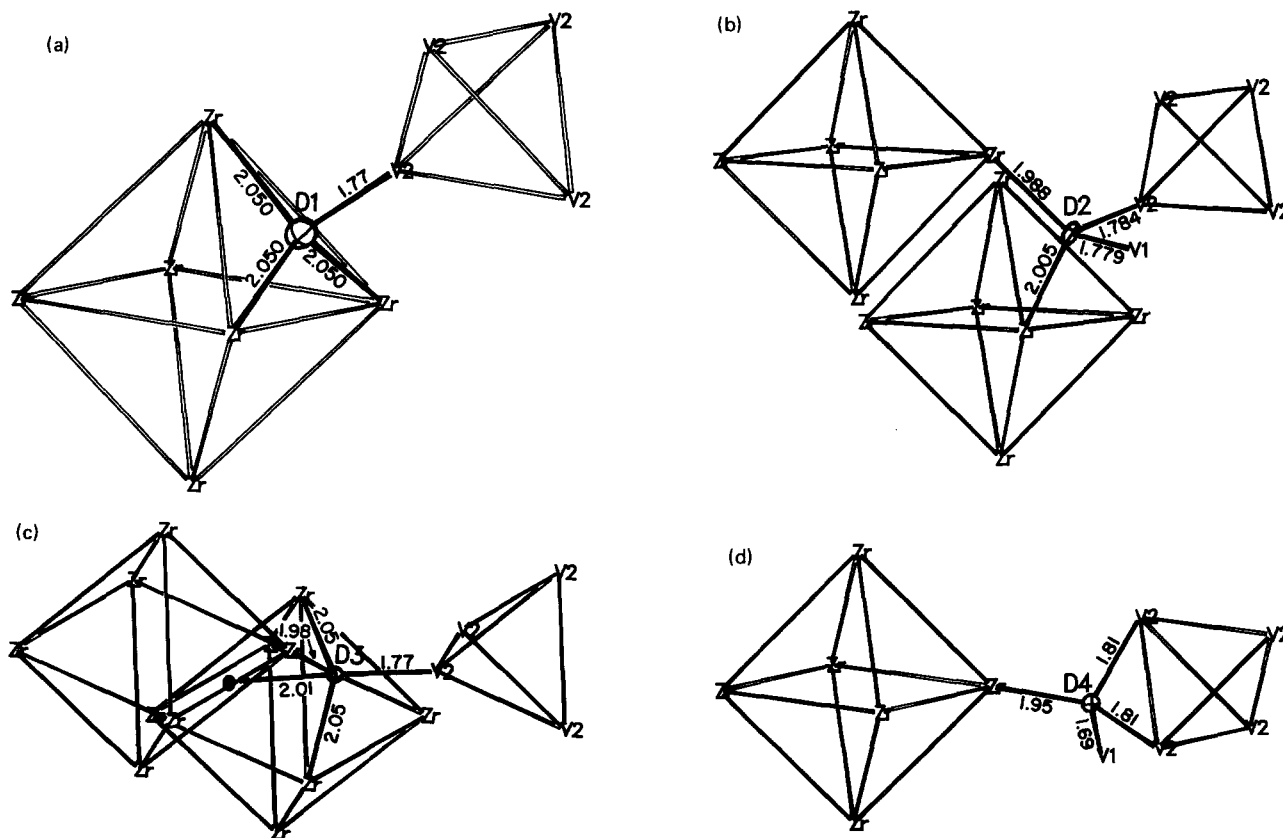


FIG. 3. Environments of deuterium atoms in  $Zr_3V_3OD_{4.95}$  (ORTEP-II drawings, 50% equiprobability thermal ellipsoids); analogous distances for the other two deuterides can be found in Table III. (a) D1 environment; (b) D2 environment; (c) D3 environment; and (d) D4 environment.

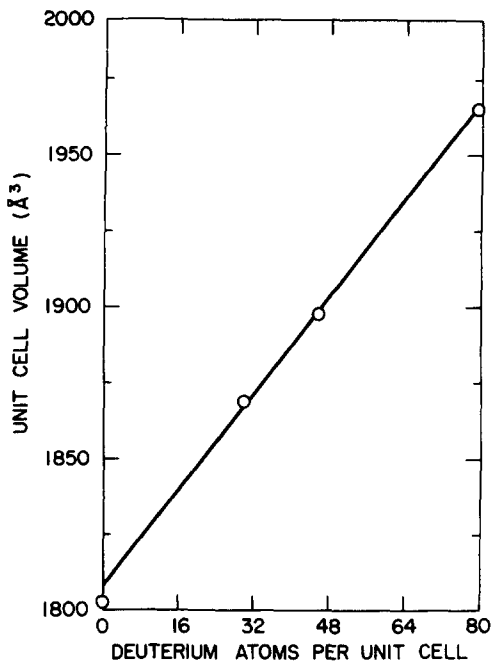


FIG. 4. Unit cell volume vs number of deuterium atoms per unit cell in  $Zr_3V_3OD_x$ . The straight line is a linear regression fit to the three points representing the deuteride phases only and has a slope of  $1.97 \text{ \AA}^3$  per deuterium atom.

pancies show that 96% of the deuterium in the structure is in the D1 site (Table V). As the D1 site fills, V1–V2 and V2–V2 distances decrease, while the Zr octahedra grow (Table IV).

The D2 site is coordinated by two zirconium atoms in separate regular Zr octahedra, one V1 and one V2 (Fig. 3). This places D2 about  $2.17 \text{ \AA}$  from D1 sites, which are almost entirely occupied when D2 begins filling (Table V). Even though 12 D2 sites per formula unit are present in the structure, impossibly short D2–D2 distances (less than  $2.1 \text{ \AA}$ ; see Table IV) limit the maximum occupation to three.<sup>14</sup> Thus in  $Zr_3V_3OD_{4.93}$ , we see that almost all of available D2 sites are filled before D3 and D4 show appreciable occupation. As D2 fills, both the Zr octahedra and the V tetrahedra expand (Table IV).

The D3 and D4 sites are occupied only slightly, even at the highest concentration studied (Table V). D3 is coordinated by three zirconium atoms and one vanadium atom and also has an oxygen near neighbor at a distance of  $2.01(5) \text{ \AA}$ . Even in the presence of a nearby oxygen atom, the D3 site maintains a coordination geometry which is approximately tetrahedral relative to Zr and V2 (Table IV). D4 is coordinated by three vanadium atoms and one zirconium atom (Fig. 3). It is unclear

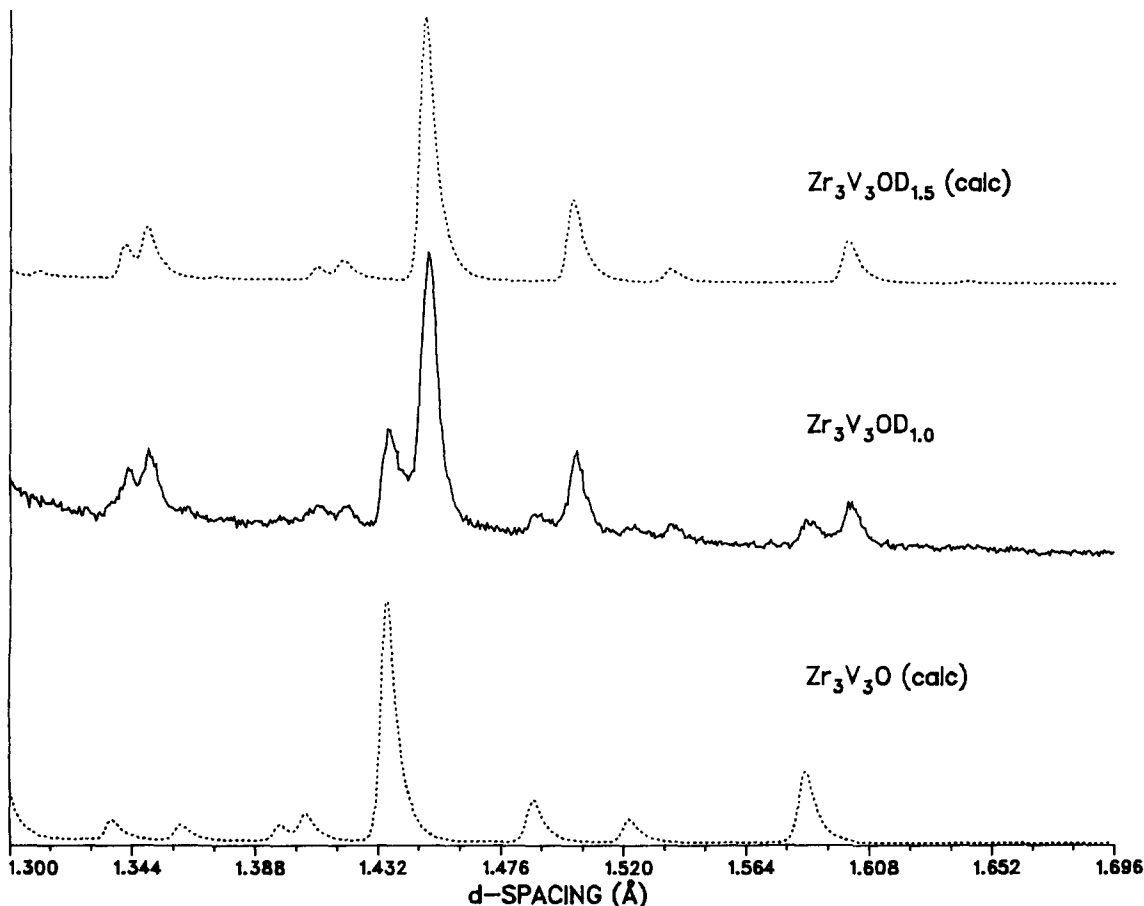


FIG. 5. Comparison of raw neutron diffraction data collected on a sample of  $Zr_3V_3OD_{1.05}$  with simulated spectra of  $Zr_3V_3O$  and  $Zr_3V_3OD_{1.5}$  (all deuterium in D1 site) over the range  $1.3 < d < 1.7 \text{ \AA}$ . The simulated spectra were calculated using the Fortran routine TOFSIMU by Rotella and Sabine (Ref. 18) with appropriate unit cell and peak shape parameters; the two simulated spectra represent an equivalent number of unit cells. The figure shows that  $Zr_3V_3OD_{1.05}$  is a mixture of  $Zr_3V_3O$  and  $Zr_3V_3OD_{1.5}$  in an approximate ratio of 1 : 2.

what role the presence of deuterium in such small amounts in the D3 and D4 sites plays in the expansion of the Zr octahedra and V2 tetrahedra from the 2.85 to the 4.93 deuteride (Table IV).

The unit cell volume increases linearly with total deuterium concentration over the range studied, in accordance with Peisel's rule<sup>15</sup> (Fig. 4). The rate of expansion is approximately  $1.97 \text{ \AA}^3$  per deuterium atom. An extrapolation of the volume expansion in the deuteride phase intersects only slightly (0.4%) above the observed volume of the alloy. This linear behavior is somewhat surprising in light of the fact that the internal structural units, i. e., vanadium tetrahedra and zirconium octahedra, do not expand uniformly. (The V tetrahedra first compress as D1 fills and then expand as D2 fills.)

It appears that the deuteride phase is not stable below about  $Zr_3V_3OD_{1.5}$ . Attempts to make samples in the range of zero to 1.5 deuteriums per formula unit give two-phase samples with the x-ray and neutron patterns of one phase matching that of the pure alloy. X-ray and neutron lattice parameters and neutron intensities indicate that the second phase has a composition near  $Zr_3V_3OD_{1.5}$ . Figure 5 shows raw neutron diffraction data for a mixed phase sample with a starting composition of  $Zr_3V_3OD_{1.05}$ , compared with computer simulations of neutron data for  $Zr_3V_3O$  and  $Zr_3V_3OD_{1.5}$ , assuming that all of the deuterium is in the D1 site with the unit cell volume taken from Fig. 4. If it is assumed that the phase which appears to be pure  $Zr_3V_3O$  contains no deuterium, it is clear from the neutron data that both the peak intensities and the lattice constant of the deuteride phase in the mixed phase sample agree with a minimum stable deuterium composition of  $Zr_3V_3OD_{1.5 \pm 0.1}$ . The possibility of a small deuterium solubility in the alloy is not ruled out, however, by the neutron data.

## DISCUSSION

It is instructive to compare the  $Zr_3V_3OD_x$  structure with that of the Laves-phase hydride  $ZrV_2D_x$ . In the Laves phase, two tetrahedrally coordinated sites are occupied by deuterium.<sup>16,17</sup> The most favored is a  $Zr_2V_2$  tetrahedron; the second site is a  $ZrV_3$  tetrahedron. Distances from deuterium to zirconium and vanadium are very similar to those observed in  $Zr_3V_3OD_x$ . Thus, qualitatively, it is evident that the most energetically favored deuterium sites are those with the largest number of zirconium neighbors, unless their occupation is hindered by a deuterium atom or oxygen atom in a near-neighbor site (e. g., D3 in

$Zr_3V_3OD_x$ ). A more detailed model for explaining deuterium site occupancy in  $Zr_3V_3OD_x$  is given in a companion paper.<sup>14</sup>

## ACKNOWLEDGMENTS

This work was supported by the U. S. Department of Energy, Office of Basic Energy Sciences. The authors wish to thank M. H. Mendelsohn for useful scientific discussions concerning previous work on  $\eta$ -carbides and their hydrides.

- <sup>1</sup>M. H. Mendelsohn, Proceedings of the 4th World Hydrogen Energy Conference, June 13–17, 1982, Pasadena, CA (in press).
- <sup>2</sup>M. V. Nevitt in *Electronic Structure and Alloy Chemistry of Transition Elements*, edited by P. A. Beck (Wiley, New York, 1963), p. 101.
- <sup>3</sup>M. H. Mueller and H. W. Knott, *Trans. AIME* **227**, 674 (1963).
- <sup>4</sup>V. H. Buchner, M. A. Gutjahr, K.-D. Beccu, and H. Skaufferer, *Z. Metallkunde* **63**, 497 (1972).
- <sup>5</sup>C. Stioui, D. Fruchart, A. Rouault, R. Fruchart, E. Roudaut, and J. Rebière, *Mat. Res. Bull.* **16**, 869 (1981).
- <sup>6</sup>T. C. Jones, T. K. Halstead, and K. H. J. Buschow, *J. Less-Common Met.* **73**, 209 (1980).
- <sup>7</sup>A. O. Cook, *J. Am. Chem. Soc.* **69**, 331 (1947).
- <sup>8</sup>B. S. Brown, J. M. Carpenter, J. D. Jorgensen, D. L. Price, and W. A. Kamitakahara in *Novel Materials and Techniques in Condensed Matter*, edited by G. Crabtree and P. Vashishta (Elsevier-North-Holland, New York, 1982); p. 311.
- <sup>9</sup>H. M. Rietveld, *J. Appl. Crystallogr.* **2**, 65 (1969).
- <sup>10</sup>R. B. VonDreele, J. D. Jorgensen, and C. G. Windsor, *J. Appl. Crystallogr.* **15**, 581 (1982).
- <sup>11</sup>E. Parthe, W. Jeitschko, and V. Sadagopan, *Acta Crystallogr.* **19**, 1031 (1965).
- <sup>12</sup>J. J. Didisheim, Ph.D. thesis, University of Geneva, Geneva, Switzerland, 1981 (unpublished) (quoted with permission of the author).
- <sup>13</sup>*International Tables for X-ray Crystallography* (Kynoch, Birmingham, England, 1974), Vol. IV; see Table 4.2, pp. 288–292.
- <sup>14</sup>D. G. Westlake, *J. Chem. Phys.* **79**, 4532 (1983).
- <sup>15</sup>H. Peisl, in *Hydrogen in Metals I, Topics in Applied Physics*, edited by G. Alefeld and J. Völkl (Springer, Berlin, 1978), Vol. 28, p. 53.
- <sup>16</sup>J.-J. Didisheim, K. Yvon, D. Shaltiel, P. Fischer, P. Bujard, and E. Walker, *Solid State Commun.* **32**, 1087 (1979).
- <sup>17</sup>D. Fruchart, A. Rouault, C. B. Shoemaker, and D. P. Shoemaker, *J. Less-Common Met.* **73**, 363 (1980).
- <sup>18</sup>F. J. Rotella and T. M. Sabine, Program and Abstracts, 32nd Annual Denver X-ray Conference and American Crystallographic Association Meeting, Snowmass, Co., 1983, p. 51.